RESEARCH ON OPTOELECTRONIC MECHANISMS FOR SEMICONDUCTOR LASERS BASED ON GaN, $Ga_xIn_{1-x}N$ and $Al_xGa_{1-x}N$ EPITAXIAL LAYERS

FINAL PROGRESS REPORT

H. C. CASEY, JR.

U.S. ARMY RESEARCH OFFICE

CONTRACT NUMBER DAAH04-96-1-0076

Duke University

APPROVED FOR PUBLLIC RELEASE

DISTRIBUTION UNLIMITED

Research on Optoelectronic Mechanisms for Semiconductor Lasers Based on GaN, $Ga_xIn_{1-x}N$ and $Al_xGa_{1-x}N$ Epitaxial Layers

Contents

Abstract 3

1. Statement of Problem 3

2. Summary of Most Important Results 4

2.1 Secondary Ionization Mass Spectrometry Standards and Measurements 4

2.2 Energy Gap of GaN 5

2.3 Optical Properties of Heavily Mg-Doped $Al_{0.09}Ga_{0.91}N$ 5

2.4 Refractive Indices of $Al_xGa_{1-x}N$ 8

2.5 Optical Field Calculations for $AlxGa_{1-x}N/In_xGa_{1-x}N$ Laser Diodes 9

2.6 Carrier Capture Times in $In_xGa_{1-x}N$ Multiple Quantum Wells 11

2.7 Collaboration with Industry 14

3. List of Publications 15

4. List of Participating Personnel 15

5. Report of Inventions 15

6. Bibliography 15

RESEARCH ON OPTOELECTRONIC MECHANISMS FOR SEMICONDUCTOR LASERS BASED ON GaN, $Ga_xIn_{1-x}N$ AND $Al_xGa_{1-x}N$ EPITAXIAL LAYERS

Abstract

The goal of this research is to understand and measure parameters that determine threshold currents and quantum efficiencies of injection lasers based on the group-III nitride solid solutions. Standards for SIMS analysis for the common impurities in the group-III nitrides were established in collaboration with Evans East. Impurity and solid solution profiles for commercial LEDs and experimental semiconductor lasers were made. The energy gap of GaN at 300 K was established as 3.452 eV. The absorption coefficient, α, and the ordinary refractive index, n_o, were obtained from optical transmission measurements of p-type $Al_xGa_{1-x}N$ doped with Mg. The dispersion of the ordinary and extraordinary refractive indices of $Al_xGa_{1-x}N$ were determined by a prism coupling technique. An algorithm was developed to permit optical field calculations for waveguiding. These calculations demonstrated that layers outside the SCH waveguide strongly affect the optical field for thin cladding layer thicknesses and result in resonant coupling of light out of the waveguide and increase the laser threshold. The electron capture time in $In_xGa_{1-x}N$ multiple quantum wells was measured to be 310-540 fs.

1. Statement of Problem

Success in the commercialization of green and blue light-emitting diodes by the Nichia Chemical Industries in Japan in the mid 1990's demonstrated the viability of optoelectronic devices based on the binary and ternary solid solutions of Al, Ga, and In with N. Because these group-III nitrides are ionic solids with the hexagonal wurtzite lattice rather than covalent solids with the zinc-blende lattice of the group-III arsenide and phosphides, the electronic and optoelectronic behavior of the nitrides differs from the arsenides and phosphides. Many properties of the group-III nitrides such as the energy gaps and the refractive indices were not known. The behavior of acceptors in the group-III nitrides was not well understood. This lack of basic knowledge has made it difficult to design and fabricate optoelectronic devices such as lasers and detectors. Control of the threshold current density requires knowledge of the gain and various losses. The losses include carrier losses due to nonradiative recombination and loss of carriers from the active region, and losses related to optical waveguiding. Heating due to excessive voltage at current densities necessary for gain emerged as a significant problem. At the end of 1996, room-temperature continuous-wave operation of InGaN multi-quantum well structure laser diodes were reported,[1] and long-lived devices are being sold in limited quantities by Nichia in Japan. Although several laboratories in both Japan and the US have reported room-temperature pulsed laser operation and rather limited operating life cw operation, no other group has been able to approach the Nichia laser results. Thus, general knowledge of the necessary growth techniques and the suitable layer structures to achieve long-lived cw room temperature operation remains an outstanding problem.

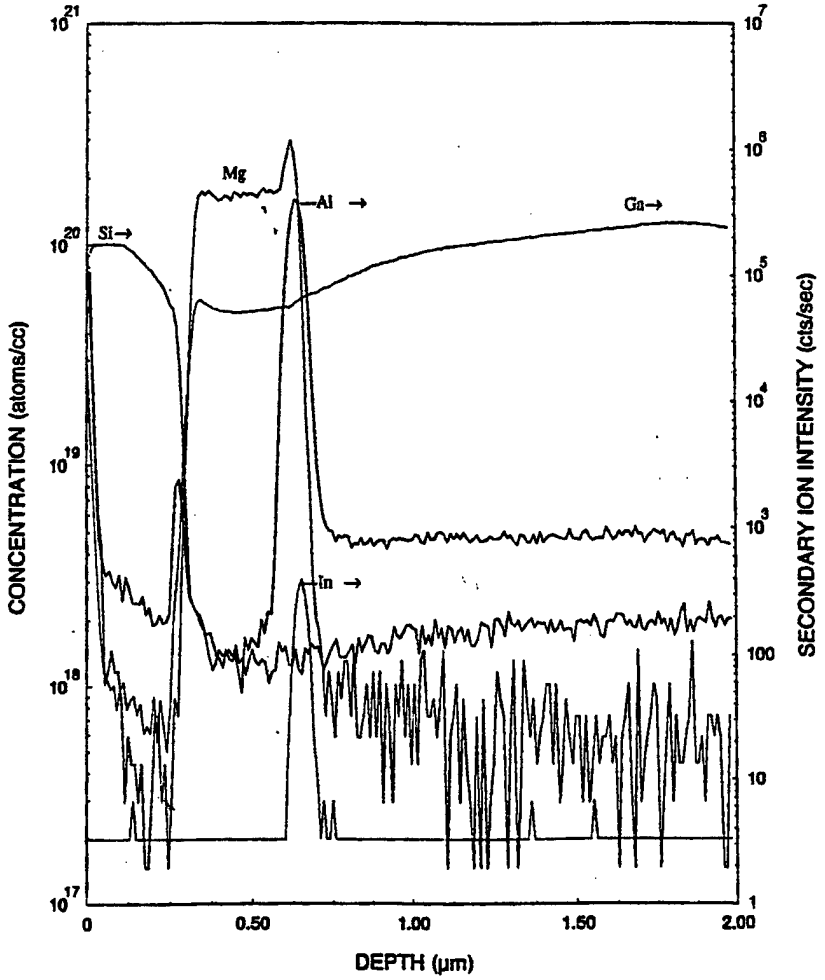

Figure 1: SIMS analysis on a blue-emitting LED grown by metalorganic chemical deposition.

2. Summary of the Most Important Results

2.1 Secondary Ionization Mass Spectrometry Standards and Measurements

Secondary Ionization Mass Spectrometry (SIMS) standards were prepared by by ion implantation in collaboration with Evans East. Standards were prepared for ^{2}H, ^{13}C, ^{18}O, ^{30}Si in GaN and AlN, and ^{25}Mg in GaN. The SIMS measurement of a blue-emitting LED with a superlattice $In_xGa_{1-x}N$ active layer is shown in Fig. 1, while the SIMS analysis for a laser structure is shown in Fig. 2. The Mg profile is plotted in atoms/cm^3 with respect to the left vertical axis. These data show that the Mg doping is about 1.7×10^{20} cm^{-3} for the LED. The Si, Ga, Al and In profiles are plotted in intensity units (counts/s) with respect to the right vertical axis. The Si at the surface for the LED is probably due to an SiO_2 layer used in patterning the LED. The results shown in Figs. 1 and 2 demonstrate that SIMS can provide the spatial resolution and the sensitivity to permit detailed quantitative information on the structures grown for optoelectronic devices. This information is essential for control of structures grown by MOCVD.

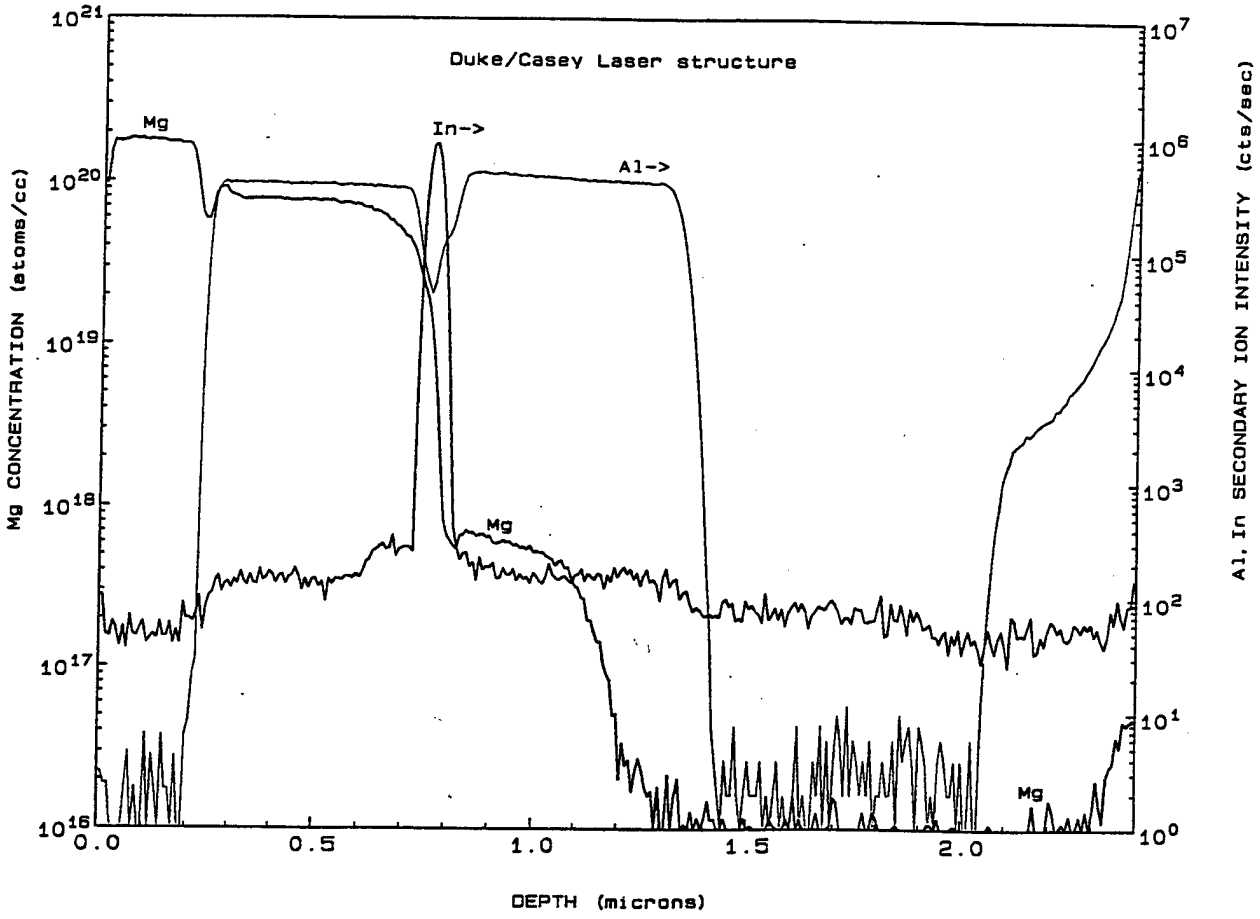

Figure 2: SIMS analysis on group-III nitride laser structure grown by metalorganic chemical deposition.

2.2 Energy Gap of GaN

Transmission measurements were made on GaN layers grown on sapphire substrates. These measurements permitted obtaining several fundamental parameters. Careful fitting the resulting absorption spectrum permitted assignment of the energy gap of lightly doped GaN at room temperature as 3.452 ± 0.001 eV, and the binding energies of the A and B excitons were determined to be $E_x^{A,B} = 20.4 \pm 0.5$ meV, and the C exciton binding energy was $E_x^C = 23.4 \pm 0.5$ meV.[2] These measurements clarified the existing uncertainty of the value of the absorption coefficient at the energy gap as $\sim 8 \times 10^4$ cm^{-1}. The measured photoluminescence spectrum agrees with the spectrum calculated from the van Roosbroeck-Shockley relation which relates the absorption coefficient to the spontaneous emission spectrum and verifies that the shape of the absorption coefficient is correct. The absorption coefficient for GaN is shown in Fig. 3. The energy gap is needed to calculate numerous basic properties of GaN, including the gain. Also, the absorption coefficient as a function of wavelength is needed in calculations involving photodetectors.

2.3 Optical Properties of Heavily Mg-Doped $Al_{0.09}Ga_{0.91}N$

In nitride-based laser diodes (LDs), $Al_xGa_{1-x}N$ is used as cladding layers to provide carrier and optical confinement. In order to achieve low resistivity p-type cladding layers,

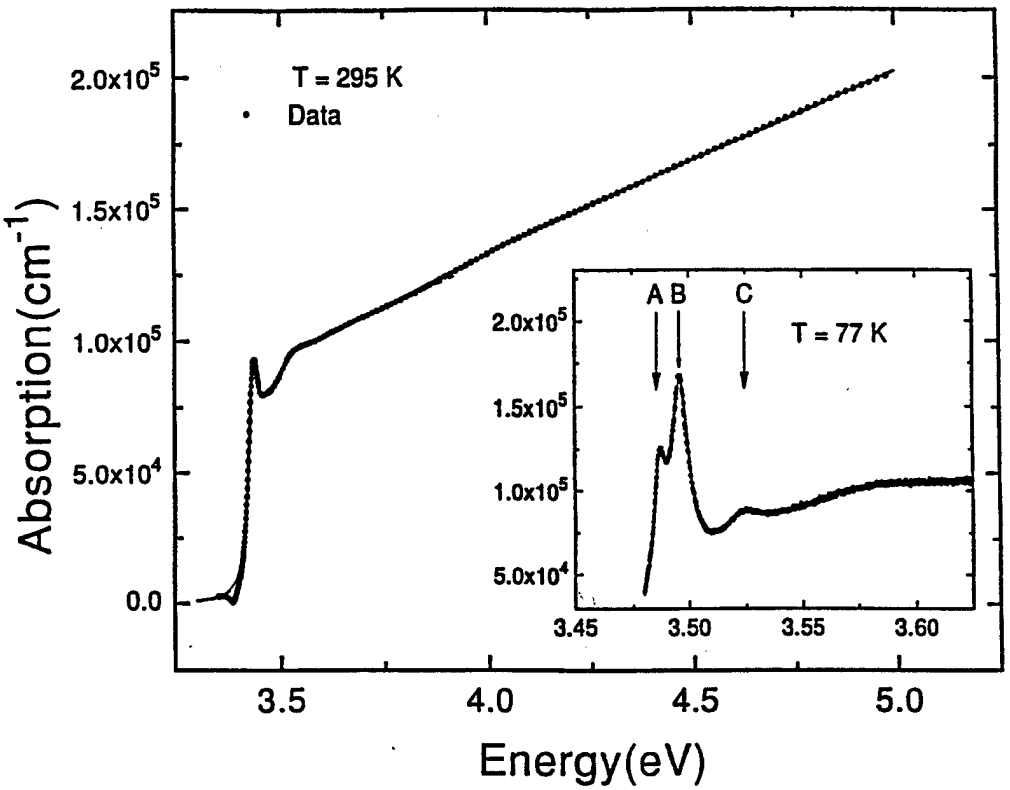

Figure 3: Absorption spectrum for GaN at room temperature. The insert is an expanded view of the excitonic structure at 77 K. At room temperature, the A and B excitonsfflerlap due to phonon broadening to form one peak while the C exciton appears as a change in slope. At 77 K, the A, B, and C excitons are clearly resolved which shows the excitonic absorption due to the three valence bands (Ref. 2).

which minimize heating of the LDs, high doping levels are needed, with doping levels of the acceptor Mg in the 19^{19}-10^{20} cm^{-3} range which results in resistivities of 1.0 Ω cm in GaN. The effects of such high doping levels on the optical properties of the cladding layers are important in LDs due to the penetration of the optical field into the cladding layers.

The optical transmission spectrum of an $Al_{0.09}Ga_{0.91}N$ epitaxial layer 0.4 μm thick with a Mg concentration of 5×10^{19} cm^{-3} as determined by SIMS is shown in Fig. 4.[3] The $Al_{0.09}Ga_{0.91}N$:Mg film and buffer layer produced a modulation of the optical transmission spectrum through interference of multiple reflections from the boundaries of the layers. The optical transmission data in Fig. 4 (solid line) is inconsistent with the model of a single thin film on a thick substrate that has been used to extract refractive index $n(\lambda)$ and absorption coefficient $\alpha(\lambda)$ from transmission data. The reduction in magnitude of the interference fringes that is most pronounced for $\lambda \approx$600 nm cannot occur in a model of a single uniform film, nor can the increase in magnitude of the local minima be accounted for. The most likely source of the modulation is a second thin layer, namely the AlN buffer layer. The matrix formulation of boundary conditions for the electric fields at the layer interfaces was used to calculate the transmittance $T(\lambda)$ of the air-film-buffer-substrate-air stack. The calculated transmittance with this analysis is the dotted line shown in the inset of Fig. 4. The importance of including the buffer layer is illustrated by comparing the agreement between

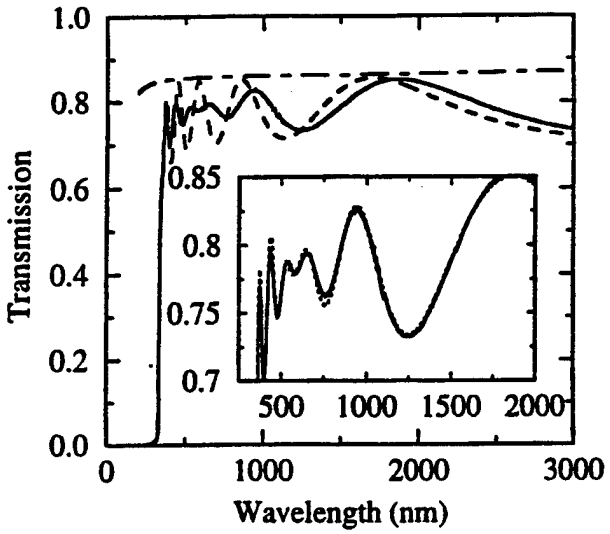

Figure 4: Transmission spectrum at room temperature for an $Al_{0.09}Ga_{0.91}N$:Mg film on a sapphire substrate with an AlN bufferlayer. The solid line is the transmission data, the dashed line is the calculated transmission spectrum with no buffer layer. The dot-dashed line is the interference-free transmission calculated for the sapphire substrate alone. In the inset, the dotted line is the fitted transmission with a buffer layer thickness of 69.7 nm (Ref. 3).

the dotted line and the transmission in the inset to that of the dashed line and the transmission in the main area of Fig. 1. Without the buffer layer, the observed "pinching" of the transmittance spectrum cannot be explained.

The dispersion of $n(\lambda)$ shown in Fig. 5(a) is in reasonable agreement with the measurement of undoped $Al_{0.11}Ga_{0.89}N$ by Brunner et al.[4] given the uncertainties in the determination of the Al composition. A second independent measurement of $n(\lambda)$ was performed by coupling light from Ar^+, HeNe, and semiconductor lasers into the film layer (waveguide layer) via a TiO_2 prism. The coupling data are indicated by filled circles in Fig. 5(a) and show good agreement with $n(\lambda)$ as determined by the transmission fit. Figure 5(b) compares the refractive index for the AlAs buffer layer to the dispersion for crystalline AlN,[4] and the low value of the buffer layer index may be due to the noncrystalline nature of the layer, defects and/or low density. The total thickness of the film and buffer layer was determined to be ~ 455 nm via mechanical profiling, which agrees well with the fit results.

In the region of strong absorption ($\lambda \leq 350$) nm, the interference effect was unobservable and the effect of the buffer layer was ignored. The combined results of the analyses for $\alpha(\lambda)$ in the regions of weak and strong absorptions are plotted as the solid line in Fig. 5(c), with the absorption coefficient for undoped GaN plotted for comparison.[2] The strong excitonic effect in the GaN, which resulted in the peak near the band-gap energy, was not present in the $Al_{0.09}Ga_{0.91}N$:Mg film and the slope of the absorption edge in the $Al_{0.09}Ga_{0.91}N$:Mg film was much reduced.

With the assumption of quasiequilibrium for the free charges, the reduced slope of the absorption edge prevents a peak from forming in the photoluminescence (PL) emission near

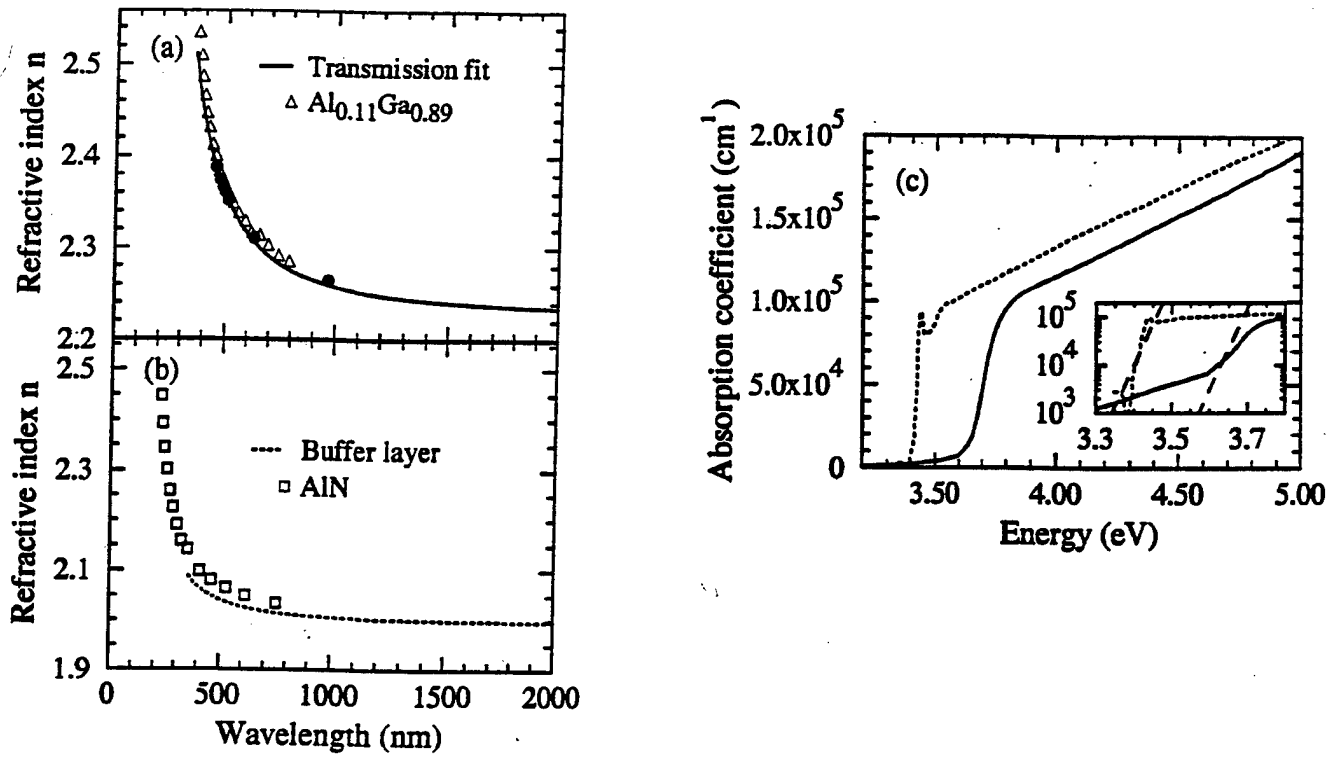

Figure 5: (a) The solid line is the ordinary refractive index of $Al_{0.09}Ga_{0.91}N$:Mg as determined by fitting to the transmission spectrum and the filled circles are determined by prism coupling. The triangles are for undoped $Al_{0.11}Ga_{0.89}N$ from Ref. 4. (b) The dotted line is the fit for the buffer layer and the squares are for undoped AlN from Ref. 4. (c) The absorption coefficients for $Al_{0.09}Ga_{0.91}N$:Mg (solid line) and undoped GaN from Ref. 2 (dotted line). The inset includes two dashed lines that are proportional to $\exp(\gamma h\nu/kT)$ Ref. 3.

the band-gap energy under continuous wave (cw) excitation. Fitting the absorption edges to an exponential function $\exp(\gamma h\nu)$ gives $\gamma \approx 80$ eV^{-1} for the GaN film and $\gamma \approx 18$ eV^{-1} for the $Al_xGa_{1-x}N$:Mg film. through the van Roosbroeck-Shockley relation, the spontaneous emission spectrum $S(h\nu)$ and $\alpha(h\nu)$ are proportional to one another[5]

$$S(h\nu) \propto (h\nu)^2 \exp(-h\nu/kT). \tag{1}$$

For a peak to appear in the spontaneous emission, $dS/d(h\nu) = 0$, requires that $\gamma \approx 1/(kT)$. The slope of the absorption edge of the $Al_{0.09}Ga_{0.91}N$:Mg film was too small to meet this condition, and under cw excitation no peak in the PL emission was detected as expected. In contrast, the GaN film had a region with a slope $\gamma \geq 1/(kT)$ and correspondingly had a PL peak. It had been an open question as to why PL could be observed for n-type $Al_xGa_{1-x}N$ but not for p-type $Al_xGa_{1-x}N$.

2.4 Refractive indices of $Al_xGa_{1-x}N$

Knowledge of the dispersion of the refractive indices of the materials is necessary for accurate modeling and design of optoelectronic devices. This need is especially true for laser diodes, where $Al_xGa_{1-x}N$ layers clad the waveguide and confine the optical field to the ac-

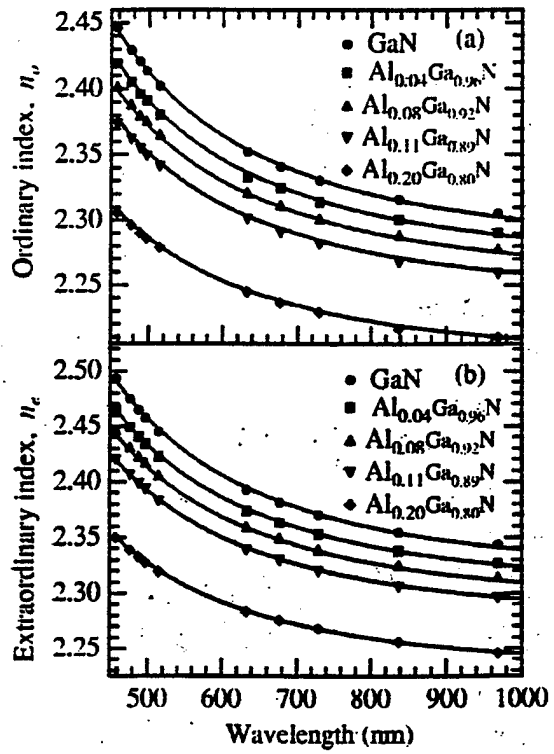

Figure 6: The ordinary (a) and extraordinary (b) refractive indices of $Al_xGa_{1-x}N$.

tive gain region. There also has been considerable discrepancy among the existing dispersion curves as a function of composition x. The wurtzite group-III nitrides lack cubic symmetry and therefore have anisotropic optical properties. The anisotropy results in uniaxial birefringence, two different refractive indices for polarization parallel and perpendicular to the c axis. The ordinary (perpendicular) $n_o(\lambda)$ and extraordinary (parallel) $n_e(\lambda)$ were measured by a prism coupling technique[6] in the wavelength range of $457 < \lambda < 980$ nm for $Al_xGa_{1-x}N$ with $x = 0.00$, 0.04, 0.08, 0.11, and 0.20.[7]

The layers were pressed against the base of a rutile TiO_2 prism. Laser light was directed through a face of the prism and focused onto the base. The lasers used were an Ar^+ ion laser (457.9, 476.5, 488, 496.5, and 514.5 nm), a HeNe laser (632.8 nm), semiconductor lasers (676.2 and 968.3 nm), and a Ti sapphire laser (729.2 and 837.3 nm). The orientation of the polarization was controlled by routing the beams through a periscope. A dielectric waveguide is formed by the $Al_xGa_{1-x}N$ film. The sapphire substrate below the film and the air above the film act as cladding layers that confine the light to the film. The resulting refractive indices are shown in Fig. 6.

2.5 Optical Field Calculations for $Al_xGa_{1-x}N/In_xGa_{1-x}N$ Laser Diodes

Relatively little has been reported on optimizing the layer design of the LDs in order to improve both the electronic and/or optical properties. A number of issues arise when considering the layer design in $Al_xGa_{1-x}NIn_xGa_{1-x}N$ LDs. For instance, the high resistivity of the p-type $Al_xGa_{1-x}N$ layers makes it desirable to grow them as thin as possible, while still maintaining good optical confinement. The proximity of a metal contact to the active

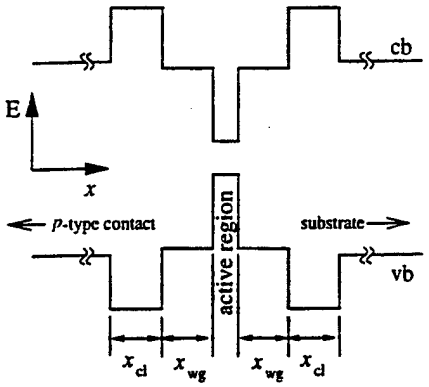

Figure 7: The conduction band (cb) and valence band (vb) in the SCH region of a LD. Structures considered here are symmetrical waveguides with x_{cl} denoting the cladding thickness and x_{wg} denoting the waveguide layer thickness (Ref. 8).

region and the presence of contacting layers with larger indices of refraction next to the active region can result in a lossy, low-confinement structure. An additional concern, in the case of a structure grown on SiC, is an absorbing substrate with a large refractive index.

The optical field interacts with the active layers to provide gain, but with the thin active region typical of nitride-based LDs most of the optical field is in the waveguide and cladding layers, which can lead to optical losses. The optical fields were calculated in asymmetrical LDs with complex refractive indices (includes the absorption coefficient) and an arbitrary number of layers for nitride-based LDs with multi-quantum well (MQW) active regions. The essential quantity for optical-field calculations is the dispersion relation for the refractive index. Refractive indices, such as those described in the previous Section, are required for these calculations. An algorithm was developed to permit optical field calculations with an arbitrary number of layers with both the refractive index and absorption.[8]

The vertical optical-field profiles were calculated[8] for many of the reported laser structures. All the LDs have the same SCH waveguide design that is shown in Fig. 7, with a MQW active region and symmetrical waveguide and cladding layers with the thicknesses x_{wg} and x_{cl}, respectively. On either side of the cladding layers, the material has a lower band-gap energy, typically GaN, which is needed for good electrical contacts. The lower band-gap material has a larger refractive index than the cladding layers and can lead to the optical field leaking out of the waveguide. The results for the LDs are shown in Fig. 8 with the relative intensity of the electric field [$\propto \mathcal{E}(x)_y^2$] given as a function of the vertical distance down from the top Au contact. The top contact is at $x = 0$ with x increasing toward the substrate. The vertical lines indicate boundaries between the layers. The horizontal open arrows indicate the region that is expanded in the inset. The inset contains the waveguide layers and the active region, where the vertical solid arrows indicate the quantum wells. The composition of the layers are indicated in the figure.

In Fig. 8(a), the intensity distribution for Nichia's LD with $\approx$ 100 h cw lifetime (structure Nichia-1)is shown.[9] The intensity distribution differs greatly from that expected for a three- or five-slab approximation to the structure because there is a significant amount of power in the GaN layer next to the Au contact. This leakage of optical power is due to the thinness

of the active region and the low (8%) Al composition in the cladding layers, which results in the electric field being coupled strongly to the optical cavity formed by the 0.3 μm GaN contact layer between the lower index layers of the $Al_{0.08}Ga_{0.92}N$ and Au.

The intensity distribution for a laser diode reported by the University of California at Santa Barbara (structure UCSB) is shown in Fig. 8(b).[10] Compared to the Nichia-1, the optical field is more confined to the active region. This results from the larger number of quantum wells (ten), the larger variation of index values (due to the longer wavelength), and the thinner (0.1 μm) GaN layer next to the Au contact. The thinner layer does not couple as strongly to the active region as does a thicker layer. The stronger confinement is reflected in the larger confinement factor (Γ) and smaller absorptive loss (α). (the confinement factor is defined as the ratio of the intensity in the quantum wells to the total intensity integrated over all x.) The optical field for the Fujitsu laser (structure Fujitsu) is shown in Fig. 8(c).[11] It is on a SiC substrate and has an optical profile similar to the Nichia-1 structure. The main difference between them is that the large refractive index of SiC causes the field from the active region to penetrate towards the substrate. note that SiC is absorbing in this wavelength region. An $\alpha = 100$ cm^{-1} was selected for the absorption coefficient in the SiC substrate, which is representative of the present high-quality wafers.

Further refinements by Nichia resulted in a laser diode with a lifetime of $>$ 3000 h that uses a superlattice (CL).[12] Figure 5(d) shows the intensity profile for this long-life LD (structure Nichia-2) with the 0.6 μm thick SL cladding layer. The optical field in this structure is more confined as compared to the field in Fig. 5(a). The reduction in thickness of the GaN layer next to the Au contact helps keep the field from coupling out of the active layer.

The confinement factors were compared for the sapphire and SiC substrates. For thin confinement layers between the active layer and the substrate, the optical field begins to reach the SiC substrate, and the large index of refraction of the SiC ($n = 2.753$) causes a strong coupling of the field into the GaN cladding layer. In the case of sapphire, with a small index of refraction ($n = 1.784$), the substrate actually helps confine the light, essentially providing a second cladding layer.

By calculating the field profile in SCH MQW LDs on sapphire and SiC substrates as a function of cladding layer and waveguide layer thicknesses, a number of design issues were considered. Optically, sapphire is preferred to SiC as a substrate material because it acts as essentially another cladding layer, due to its low index of refraction and lossless nature. In fact, the confinement factor on the sapphire substrate is found to be very insensitive to the cladding layer thickness for the range of 0.3-0.8 μm. In contrast, a SiC substrate, which is lossy and has a large index of refraction, can significantly decrease optical confinement as the cladding layer thickness is reduced. For the confinement factor in a LD on SiC to be comparable to that for a LD on sapphire, $x_{cl} \geq 0.6$ μm. These calculations also demonstrated the resonant features in the properties of the waveguides due to the coupling of the optical field into the thick GaN contact layer on the n side of the LD.

2.6 Carrier Capture Times in $In_xGa_{1-x}N$ Multiple Quantum Wells

Sub-picosecond wavelength-degenerate differential transmission optical spectroscopy was used to characterize the electron capture time in $In_xGa_{1-x}N$ multiple-quantum well (MQW)

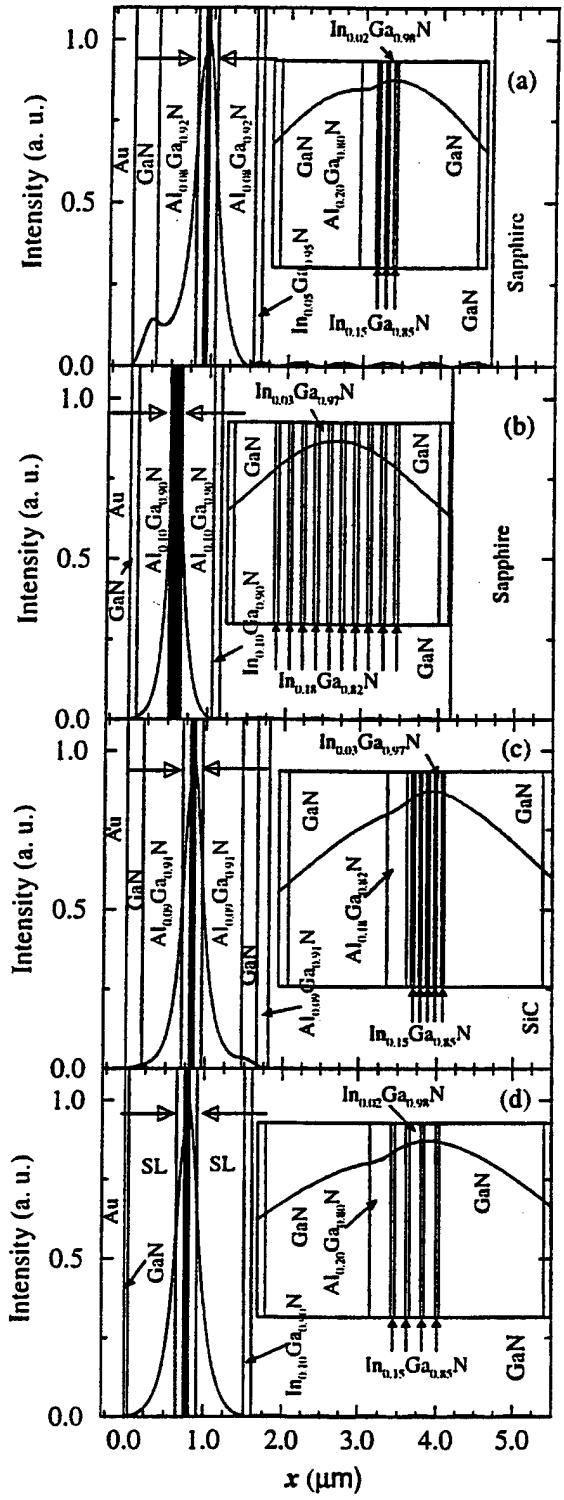

Figure 8: Optical-field intensities for reported lasing MQW SCH LDs: (a) Nichia-1, (b) UCSB (c) Fujitsu (d) Nichia-1. The vertical lines indicate layer boundaries. The insets show the active and waveguiding layers (the region indicated by the horizontal open arrows), with the vertical solid arrows pointing to the quantum wells.

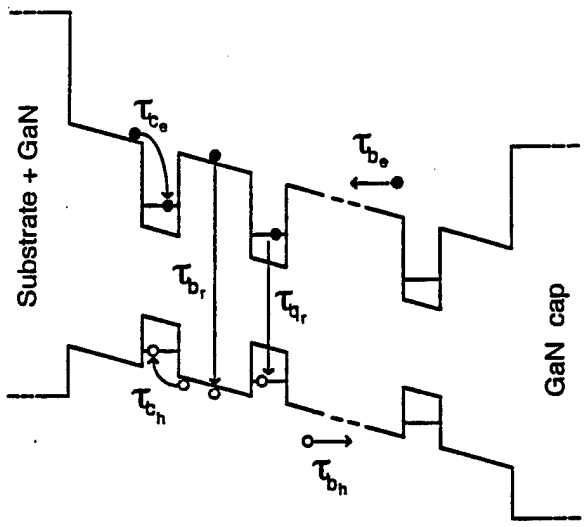

Figure 9: Schematic representation of the multiple-quantum well structure used in the capture time measurements. The quantities τ_{c_e} and τ_{c_h} represent the electron and hole capture times. The recombination times in the wells are represented by τ_{q_r} and τ_{b_r}. Transport times across the confining GaN layers are τ_{b_e} and τ_{b_h}.

structure.[13] Quantum-well lasers have complex structures such as those illustrated in Fig. 9 with wider energy gap layers for carrier confinement with three-dimensional (bulk) properties which are coupled to two-dimensional quantum wells. The capture time becomes significant because it effects the flow of carriers into the quantum wells. This capture rate must be as fast as the the carrier removal rate due to stimulated emission. In lasers, The inability of carriers to relax quickly enough into the quantum wells can decrease the gain and the differential quantum efficiency.

The sample was grown by metalorganic chemical deposition (MOCVD) at the University of California at Santa Barbara in a modified two flow reactor on double polished c-plane sapphire. It consists of a 10-period MQW with 25 Å $In_{0.15}Ga_{0.85}N$ wells and 55 Å $In_{0.05}Ga_{0.85}N$ barriers doped with Si. There is a 0.1 μm GaN cap layer on top of the MQW, and the structure is grown on top of a $\sim$ 2 μm GaN layer doped with Si. The Si doping is $\sim 10^{18}$ cm^{-3}. This structure is similar to those used in lasers.

To measure the carrier capture time, standard wavelength-degenerate differential transmission (DT) spectroscopy was performed with a mode-locked Ti:Sapphire (Ti:S) laser with external frequency doubling. Following a 1 μm resolution stepper motor provided 7 ps time resolution between between the pump and probe. The beams were overlapped on the sample with an incident angle approximately 5° from normal, and the pump beam was defocused to a spot diameter (100 μm) roughly 2.5 times larger than the probe beam to ensure uniform illumination of the probed region. The cross-polarized probe beam was passed through a polarizer to eliminate stray pump light on the high-speed Si photodetector, while the pump beam was varied in intensity with a variable reflector wheel and chopped at 2 kHZ to permit lock-in detection.

Relative to the 3.22 eV barrier energy, typical data for excitation above (3.262 eV), near

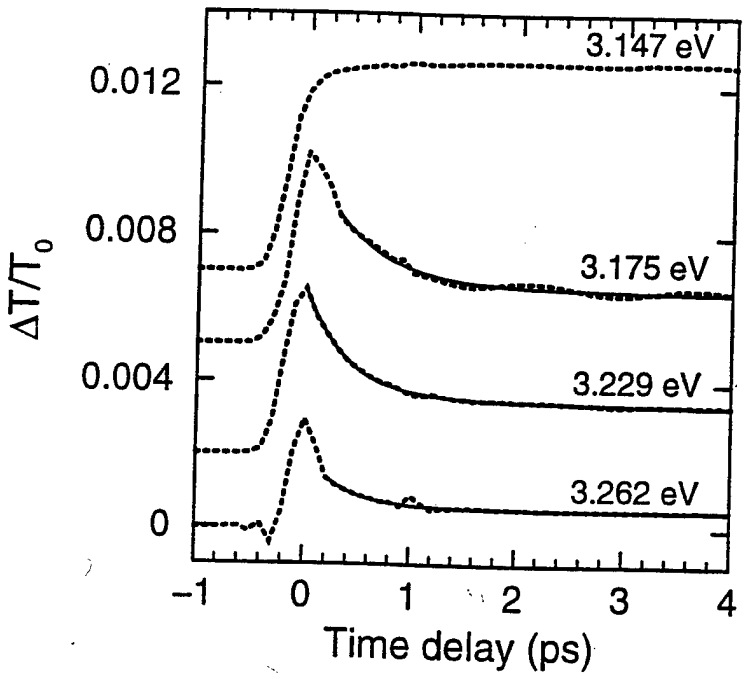

Figure 10: Normalized, time-resolved 14 DT data for the InGaN smaple, overlaid by the bi-exponential fit, for four different pump/probe energies.

(3.229 eV and 3.175 eV), and below (3.147 eV) the barrier are shown in Fig. 11. The feature at $\sim$ 1 ps corresponds to a reflection Artifact and should be ignored. Over a range of pump/probe energies near the barrier energy (3.169-3.262 eV), the data have similar shape, revealing a fast (f), sub-ps decay and a much slower (s), sub-ns decay. The decay portion of the DT data was fit with a simple bi-exponential: $A_f \exp(-t/\tau_f) + A_s \exp(-t/\tau_s)$. The features were significantly slower than the 85 fs pump/probe pulse. The 310-540 fs t_f values represent electron capture from the 3D barrier states to the 2D QWs. The slower decay feature was strongly dependent on the excitation wavelength and varies from 300 ps to as fast as 20 ps, and different relaxation mechanisms must be occurring such as non-radiative recombination.

2.7 Collaboration With Industry

During the time period of this contract, collaboration was established with Cree Research, which was also a DARPA contractor. Results such as the program for calculating the optical fields in laser structures were made available to Cree. A National Science Foundation (NSF) program made possible the continuation of the postdoctoral Research Associate on this project through the Grant Opportunity for Academic Liaison with Industry (GOALI) program. The postdoctoral Research Associate was then partially funded by the NSF GOALI Grant and funding from Cree Research. Therefore, the experience gained on this DARPA grant made it possible for the postdoctoral Research Associate to continue the group-III nitride laser work at a company committed to develop a commercial blue laser.

3. List of Publications

1. J. F. Muth, J. H. Lee, I. K. Shmagin, R. M. Kolbas, H. C. Casey, Jr., B. P. Keller, U. K. Mishra, and S. P. DenBaars, " Absorption Coefficient, Energy Gap, Exciton, Binding Energy, and Recombination Lifetime of GaN Obtained from Transmission Measurements," Appl. Phys. Lett. **71**, 2572 (1997).

2. M. J. Bergmann and H. C. Casey, Jr., "Optical-Field Calculations for Lossy Multiple-Layer $Al_xGa_{1-x}N/In_xGa_{1-x}$ Laser Diodes," J. Appl. Phys. **84**, (1998).

3. M. J. Bergmann, Ü. Özgür, H. C. Casey, Jr., J. F. Muth, Y. C. Chang, R. M. Kolbas, R. A. Rao, C. B. Eom, and M. Schurman, "Linear Optical Properties of a Heavily Mg-Doped $Al_{0.09}N$ Epitaxial Layer," Appl. Phys. Lett. **74**, 3188 (1999).

4. M. J. Bergmann, Ü. Özgür, H. C. Casey, Jr., H. O. Everitt, and J. F. Muth, "Ordinary and Extraordinary Refractive Indices for $Al_xGa_{1-x}N$ Epitaxial Layers," Appl. Phys. Lett. **75**, 67 (1999).

5. C. W. Teng, J. F. Muth, Ü. Özgür, M. J. Bergmann, H. O. Everitt, A. K. Sharma, C. Jin, and J. Narayan, "Refractive Indices and Absorption Coefficients of $Mg_xZn_{1-x}O$ Alloys," Appl. Phy. Lett. **76**, 979 (2000).

6. Ö. Üzgür, M. J. Bergmann, H. C. Casey, Jr., and H. O. Everitt, "Ultrafast Optical Characterization of Carrier Capture Times in $In_xGa_{1-x}N$ Multiple Quantum Wells," Appl. Phys. Lett. (in press).

4. List of Participating Personnel

H. C. Casey, Jr., Professor of Electrical and Computer Engineering
M. J. Bergmann, Research Associate, Departments of Electrical and Computer Engineering and Physics

5. Report of Inventions

A patent disclosure has been made for a process for removal of hydrogen from Mg-doped group-III nitride layers which does not depend on heating for out-diffusion of hydrogen.

6. Bibliography

1. S. Nakamura, M. Senoh, S. Nagahama, N. Iwasa, T. Yamada, T. Matsushita, Y. Sugimoto and H. Kiyoku, Appl. Phys. Lett. **69**, 4056 (1996).

2. J. F. Muth, J. H. Lee, I. K. Shmagin, R. M. Kolbas, H. C. Casey, Jr., B. P. Keller, U. K. Mishra, and S. P. DenBaars, Appl. Phys. Lett. **71**, 2572 (1997).

3. M. J. Bergmann, Ü. Özgür, H. C. Casey, Jr., J. F. Muth, Y. C. Chang, R. M. Kolbas, R. A. Rao, C. B. Eom and M. Schurman, Apl. Phys. Lett. **74**, 3188 (1999).

4. D. Brunner, H. Angerer, E. Bustarret, F. Freudenberg, R. Höpler, R. Dimitrov, O. Ambacher and M. Stutzmann, J. Appl. Phys. **82**, 5090 (1997).

5. W. van Roosbroeck and W. Shockley, Phys. Rev. **94**, 1558 (1954).

6. P. K. Tien, R. Ulrich, and R. J. Martin, Appl. Phys. Lett. **14**, 291 (1969).

7. M. J. Bergmann, Ü. Özgür, H. C. Casey, Jr., H. O. Everitt, J. F. Muth, Appl. Phys. Lett. **75**, 67 (1999).

8. M. P. Mack, A. Abare, M. Aizcorbe, P. Kozodoy, S. Keller, U. K. Mishra, L. A. Coldren and S. P. DenBaars, MRS Internet J. Nitride Semiconductor Res. **2**, 41 (1997).

9. A. Kuramata, K. Domen, R. Soejima, K. Horino, S. Kubota and T. Tanahashi, Jpn. J. Appl. Phys., Part 2 **36**, L1130 (1997).

10. S. Nakamura et al., Appl. Phys. Lett. **72**, 211 (1998).

11. Ü. Özgür, M. B. Bergmann, H. C. Casey, Jr., and H. O. Everitt, Appl. Phys. Lett. (in press).

SF 298 MASTER COPY KEEP THIS COPY FOR REPRODUCTION PURPOSES

REPORT DOCUMENTATION PAGE

Form Approved
OMB NO. 0704-0188

1. AGENCY USE ONLY *(Leave blank)*	2. REPORT DATE	3. REPORT TYPE AND DATES COVERED
	February 10, 2000	Final Report 6/1/96 - 12/31/99

4. TITLE AND SUBTITLE
Research on Optoelectronic Mechanisms for Semiconductor Lasers Based on GaN, $Ga_xIn_{1-x}N$ and $Al_xGa_{1-x}N$

5. FUNDING NUMBERS
#DAAH04-96-1-0076

6. AUTHOR(S)
H. C. Casey, Jr.

7. PERFORMING ORGANIZATION NAMES(S) AND ADDRESS(ES)
Department of Electrical and Computer Engineering
Box 90291
Duke University
Durham, NC 27708-0291

8. PERFORMING ORGANIZATION REPORT NUMBER
HCC00-1

9. SPONSORING / MONITORING AGENCY NAME(S) AND ADDRESS(ES)
U.S. Army Research Office
P.O. Box 12211
Research Triangle Park, NC 27709-2211

10. SPONSORING / MONITORING AGENCY REPORT NUMBER
ARO 35588.7-EL

11. SUPPLEMENTARY NOTES
The views, opinions and/or findings contained in this report are those of the author(s) and should not be construed as an official Department of the Army position, policy or decision, unless so designated by other documentation.

12a. DISTRIBUTION / AVAILABILITY STATEMENT
Approved for public release; distribution unlimited.

12 b. DISTRIBUTION CODE

13. ABSTRACT *(Maximum 200 words)*

The goal of this research is to understand and measure parameters that determine threshold currents and quantum efficiencies of injection lasers based on the group-III nitride solid solutions. Standards for SIMS analysis for the common impurities in the group-III nitrides were established in collaboration with Evans East. Impurity and solid solution profiles for commercial LEDs and experimental semiconductor lasers were made. The energy gap of GaN at 300 K was established as 3.452 eV. The absorption coefficient, α, and the ordinary refractive index, n_o, were obtained from optical transmission measurements of p-type $Al_xGa_{1-x}N$ doped with Mg. The dispersion of the ordinary and extraordinary refractive indices of $Al_xGa_{1-x}N$ were determined by a prism coupling technique. An algorithm was developed to permit optical field calculations for waveguiding. These calculations demonstrated that layers outside the SCH waveguide strongly affect the optical field for thin cladding layer thicknesses and result in resonant coupling of light out of the waveguide and increase the laser threshold. The electron capture time in $In_xGa_{1-x}N$ multiple quantum wells was measured to be 310-540 fs.

14. SUBJECT TERMS	15. NUMBER IF PAGES
GaN, AlN, InN, absorption coefficient, injection lasers, LEDs, refractive indices, optical field calculations, electron capture in MQWs.	16
	16. PRICE CODE

17. SECURITY CLASSIFICATION OR REPORT	18. SECURITY CLASSIFICATION OF THIS PAGE	19. SECURITY CLASSIFICATION OF ABSTRACT	20. LIMITATION OF ABSTRACT
UNCLASSIFIED	UNCLASSIFIED	UNCLASSIFIED	UL